Advanced Sustainable Systems

ADVANCED SUSTAINABLE SYSTEMS
www.advsustainsys.com

RESEARCH ARTICLE OPEN ACCESS

Interplay of Fiber Surface Properties and Processing on the Performance of Sustainable Bamboo-Reinforced Bio-Polycarbonate Composites

Dimitrios Apostolidis[1] | Prajwal Jayaraman[1] | Baris Kumru[1,2]

[1]Aerospace Structures & Materials Department, Faculty of Aerospace Engineering, Delft University of Technology, Delft, The Netherlands | [2]School of Energy Science and Engineering (ESE), Vidyasirimedhi Institute of Science and Technology (VISTEC), Wangchan Valley, Rayong, Thailand

Correspondence: Dimitrios Apostolidis (d.apostolidis@tudelft.nl) | Prajwal Jayaraman (prajwal.jay03@gmail.com) | Baris Kumru (b.kumru@tudelft.nl)

Received: 2 October 2025 | **Revised:** 10 February 2026 | **Accepted:** 19 February 2026

Keywords: circular buildings | circular composites | natural fibre composites | renewable composites | renewable matrix

ABSTRACT

This study explores the development of sustainable bamboo fiber-reinforced bio-based polycarbonate (BF-PC) composites. Prepreg laminates were fabricated using solvent-based impregnation and compression molding. The effects of chemical surface modifications—alkali and silane—on bamboo fiber properties, interfacial bonding, and composite performance are studied and supplemented by comprehensive characterization, including FTIR, SEM, fiber density, single fiber tensile testing, cross-sectional microscopy, void fraction analysis, and tensile and flexural testing. Results revealed that 2 g/L silane-treated fibers showed the highest improvements in mechanical properties and interfacial adhesion, achieving tensile and flexural strengths of 162 MPa and 184 MPa, respectively. In contrast, alkali treatments failed to improve bonding and resulted in lower composite performance. In summary, surface chemistry of natural fibers and circular buildings, circular composites, natural fibre composites, renewable composites, renewable matrixcomposite processing play a crucial role in renewable polycarbonate matrix composite engineering.

1 | Introduction

The development of sustainable, high-performance composites is a critical focus in modern materials science, driven by increasing environmental concerns and the need to reduce reliance on fossil-based materials [1, 2]. Natural fiber-reinforced thermoplastic composites (NFRCs) have gained traction as potential alternatives to conventional composite systems. Natural fibers are renewable, biodegradable, and often require significantly lower energy inputs for production and processing. Moreover, their relatively low density and favorable specific mechanical properties make them suitable for a range of semi-structural and technical applications [3, 4]. Additionally, the sustainability of the polymer matrix is among the major factors that influence the composite circularity [5]. As for the case of thermoplastic matrices, potential for recycling and reuse render thermoplastic composites as attractive candidates for the circular composites industry [6].

Among the various lignocellulosic fibers explored, bamboo fiber stands out due to its exceptional growth rate, high cellulose content, and hierarchical structure that imparts promising mechanical performance [7]. Mechanically extracted bamboo fibers typically exhibit tensile strengths in the range of 200–500 MPa and elastic moduli above 20 GPa, depending on species, processing, and test conditions [8]. The fiber's low density (~1.3 g/cm^3), combined with its abundant availability and mechanical resilience, offers a viable route to the development of lightweight bio-composites. However, the heterogeneous surface chemistry and hydrophilic nature of bamboo fibers pose

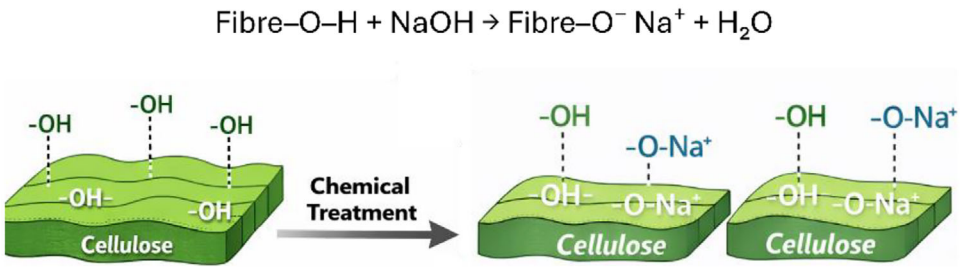

SCHEME 1 | Chemical interactions during alkali treatment of cellulosic fibers.

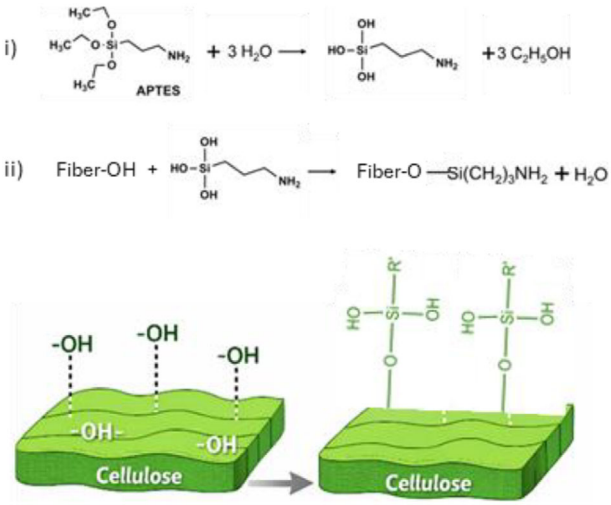

SCHEME 2 | Chemical interactions during silane treatment of cellulosic fibers.

significant challenges to effective reinforcement when embedded in polymer matrices [9, 10].

Interface properties of natural fibers are handled via surface treatments to tailor their surface energy, topography, and chemical functionality. Alkali treatment (NaOH) is a well-established method that removes amorphous constituents such as lignin and surface impurities, increases fibrillation, and roughens the fiber surface—thus promoting mechanical interlocking with the matrix [11]. However, aggressive alkali concentrations can degrade cellulose crystallinity and reduce fiber strength. Silane coupling agents, typically alkoxysilanes, react with hydroxyl groups on the fiber surface while providing matrix-reactive end groups. The resulting siloxane network enhances chemical adhesion, improves dispersion, and suppresses moisture uptake [12]. While these treatments have been widely applied in bio-composite systems, their effectiveness depends strongly on concentration, processing method, and the specific polymer matrix used [13].

Polycarbonate (PC) is an engineering amorphous thermoplastic with a favorable balance of mechanical strength, thermal stability, and ductility. It is widely used in demanding applications requiring impact resistance, dimensional accuracy, and transparency [14, 15]. The polymer backbone contains carbonate linkages, which introduce polarity, but its overall surface energy remains insufficient for spontaneous bonding with untreated natural fibers [16]. PC exhibits high melt viscosity and requires processing temperatures typically ranging from 200°C to 230°C—close to or beyond the degradation onset of most lignocellulosic fibers [17]. These factors contribute to interfacial incompatibility and hinder effective stress transfer across the fiber–matrix boundary. Additionally, studies by Zhang et al. and Maheshwari et al. have shown improved fiber-matrix adhesion between lignocellulosic fibers and polycarbonate matrix by bridging the polarity gap between them [18, 19].

In the context of polycarbonate-based NFRCs, the literature remains limited with respect to systematic evaluations of fiber surface treatments and their influence on fiber morphology, interfacial adhesion, and overall composite performance. Furthermore, due to the temperature sensitivity of natural fibers, conventional melt-processing techniques often compromise fiber integrity [20]. An emerging alternative involves the use of solvent-assisted prepreg, wherein the polymer is dissolved in a suitable solvent and impregnated into the fiber bed at low temperature [21]. After solvent evaporation, the prepregs can be consolidated via compression molding at controlled temperatures and pressures. This method facilitates improved fiber wetting and matrix distribution while mitigating thermal degradation, resulting in composites with enhanced microstructural homogeneity and reduced void content [21].

This work explores the influence of alkali and silane treatments on the morphology, chemical structure, and density of bamboo fibers, as well as their performance in polycarbonate-based composites. Treated and untreated fibers were processed into unidirectional laminates using a solvent-based prepreg method followed by compression molding. Detailed characterization was carried out at both fiber and composite levels using Fourier-transform infrared spectroscopy (FTIR), scanning electron microscopy (SEM), fiber density, single-fiber tensile testing, and mechanical testing of laminates in tension and flexure. Additional microstructural analysis included cross-sectional imaging and quantification of voids and fiber–matrix bonding efficiency.

2 | Materials

Bamboo fibers (with an average length of 21 cm and a diameter of 256.6 ± 112 mm) were supplied by Bambooder and bio-based polycarbonate resin (Durabio) sourced in pellet form from Mitsubishi Chemicals. Acetic anhydride (≥99%), perchloric acid (60%), 3-aminopropyltriethoxysilane (≥99%), sodium hydroxide

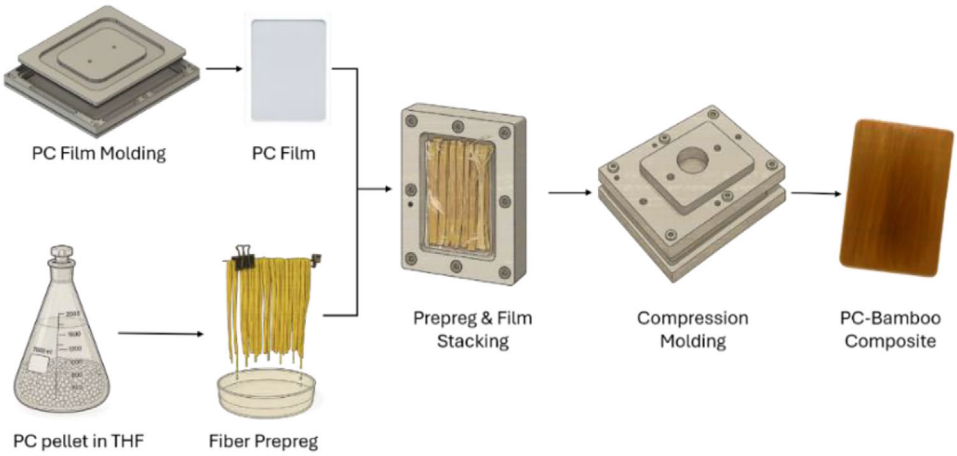

SCHEME 3 | Processing Steps for BF-PC Composite Laminate.

(≥98%, pellet form), and tetrahydrofuran (≥99%) were obtained from Merck Sigma-Aldrich. Acetic acid (≥99.8%) and denatured ethanol (96%) were sourced from the Central Warehouse of L&M. Toluene (≥99.85%) was procured from Thermo Fisher Scientific.

3 | Methodology

3.1 | Equipment

Fourier transform infrared (FTIR) measurements are performed using a Spectrum 100 Optica FT-IR Spectrometer equipped with an attenuated total reflectance (ATR) accessory and a diamond crystal. The spectra are recorded in the range of 4000 to 550 cm^{-1} with a resolution of 1 cm^{-1} and 16 scans. Data processing is carried out using Origin software. Fiber density was measured using an Anton Paar Ultrapyc 5000 helium pycnometer as per ASTM D8171—*Standard Test Method for Density Determination of Flax Fiber* [22]. Fiber surface morphology was examined using a JSM-7500F Scanning Electron Microscope (SEM). Composite sample manufacturing was performed utilizing a 1000 kN Joos hot press at 5 bar pressure at 200°C with an initial dwell at 105°C. Mechanical tests for the individual fibers and the composite samples were conducted using a 10 kN and 20 kN Universal Testing Machine (Zwick) equipped with a 100N and 20 kN load cell, respectively, at a crosshead speed of 1 mm/min. Optical images were taken using a Keyence VK-X1000 confocal scanning microscope

3.2 | Chemical Treatments

All bamboo fiber samples were pre-dried in a vacuum oven at 80°C for 1 h to eliminate surface and loosely bound moisture. For all treatments, a fiber-to-solution concentration of 60% w/v was maintained to ensure consistency in reagent exposure and treatment conditions across all batches. Following chemical treatment, all fibers were thoroughly rinsed 3–4 times with ethanol and distilled water to remove residual reagents. Rinsing was continued until a neutral pH (≈7) was reached. The fibers were then dried in a vacuum oven at 80°C for 20 h to ensure complete moisture elimination prior to subsequent characterization and composite processing.

3.3 | Alkali Treatment

Alkali treatment was performed using sodium hydroxide (NaOH) solutions at concentrations of 2%, 5%, and 8% (w/v). Solutions were prepared by dissolving NaOH in distilled water, and bamboo fibers were immersed at room temperature for 2 h. This aligns with current practices, where NaOH concentrations range from 0.5% to 10% and treatment durations from 20 min to 8 h [23–25]. The schematic showing the chemical interactions taking place during the alkali treatment of lignocellulosic fibers can be seen in Scheme 1.

3.4 | Silane Treatment

A coupling solution of 3-aminopropyltriethoxysilane (APTES) was prepared using an 80:20 (v/v) mixture of denatured ethanol and distilled water. The pH was adjusted to 5 by the addition of acetic acid and acetic anhydride to promote hydrolysis. Silane concentrations of 2, 5, and 8 g/L were employed. Bamboo fibers were immersed in each solution for 2 h at ambient temperature [12, 26, 27]. The schematic showing the chemical interactions taking place during the alkali treatment of lignocellulosic fibers can be seen in Scheme 2.

3.5 | Single Fiber Sample Preparation

Single fiber tensile testing was conducted as per the ASTM C1557—*Standard Test Method for Tensile Strength and Young's Modulus of Fibers* [28]. Individual fibers were mounted on paper tabs using an adhesive at a gauge length of 80 mm. Care was taken to select only single fibers, which were verified under a microscope. Fiber diameters were measured prior to testing to enable accurate strength calculations. The average diameter was used, as minimum or maximum values could significantly alter the results. Before testing, the fiber-tab assemblies were dried in an oven at 50°C for 30 min. Tabs were then carefully slit at the

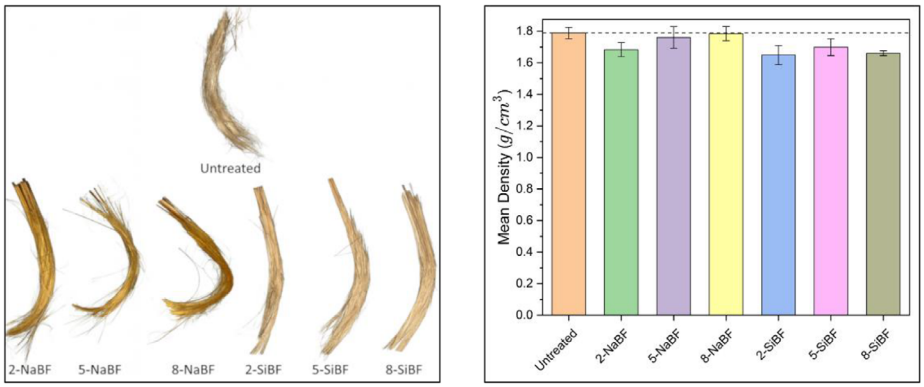

(a) Alkali and silane treated fibers showing changes in color.

(b) Skeletal density of the fibers subject to different treatments.

FIGURE 1 | (a) Images of treated Bamboo fibers, (b) their respective density.

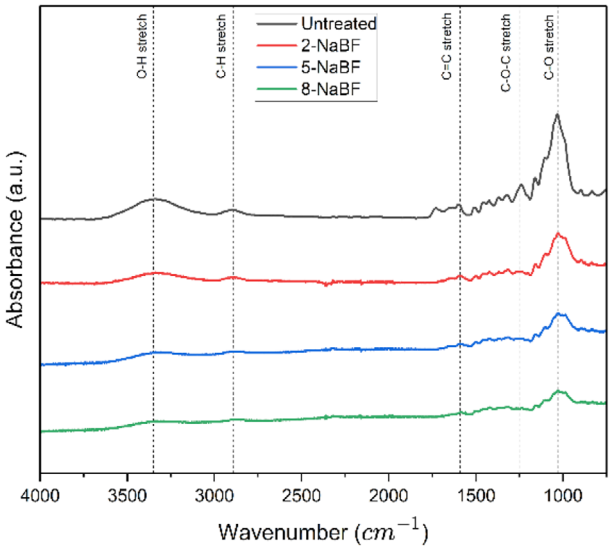

FIGURE 2 | Removal of O—H and C—H bonds of lignin between 3500 and 2750 cm^{-1} and reduction in C=C bond at ≈1600 cm^{-1}.

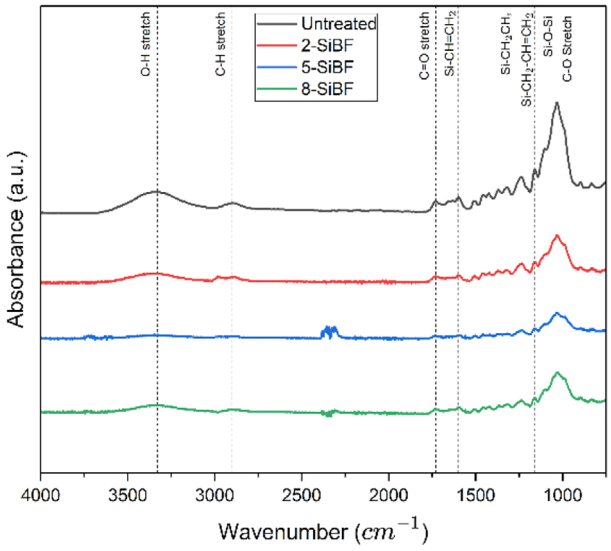

FIGURE 3 | Removal of O—H and C—H groups of lignin and presence of various Si-groups between 1750 and 1000 cm^{-1}.

center to free the gauge length. A strain rate of 0.25 mm/min was employed to capture fiber behavior. A sample size of 10 specimens was used to improve statistical reliability. The average tensile modulus, E_f, was calculated using:

$$E_f = \frac{\Delta_\sigma}{\Delta_\varepsilon}$$

where stress and strain were taken from the linear region of the force-displacement curve.

3.6 | Composite Processing

A solution-based prepreg method was employed for composite manufacturing. Acetone, initially tested for its accessibility and low toxicity [29], led to a turbid solution, indicating incomplete dissolution of the polymer. Tetrahydrofuran (THF)is then selected and achieves complete dissolution under stirring at room temperature. A saturation study determined the weight-to-weight (w/w) solubility limit of PC in THF by incrementally adding solvent to a fixed polymer mass until equilibrium, which was reached at 30 wt.% polycarbonate (PC)–THF solution Scheme 3.

Fiber bundles were pre-weighed for matrix mass fraction estimation, then arranged into unidirectional (UD) mats and fixed with tape. Stem ends were excluded from impregnation and trimmed postdrying. Fiber mats were immersed, drained, and air-dried at room temperature to allow slow solvent evaporation and afford uniform PC deposition within the fibrous network. Excess solution was recovered for reuse. After 24 h of drying, the prepregs became rigid, improving handling but limiting fiber distribution during molding. Dried prepreg mats were placed flat into the aluminum mold for consolidation. Despite fiber hardening after prepreg formation hindering perfect unidirectional alignment, an ideal UD distribution was assumed in all calculations. To achieve a 60 wt% matrix content, additional PC films were interleaved between fiber layers. The PC films were manufactured by compression-molding pellets into films using a custom aluminum mold. A predwell at 105°C facilitated moisture removal, followed by pressing at 200°C and 5 bar. This temperature was selected to prevent bamboo fiber degradation and maintain consistency in composite processing. Approximately

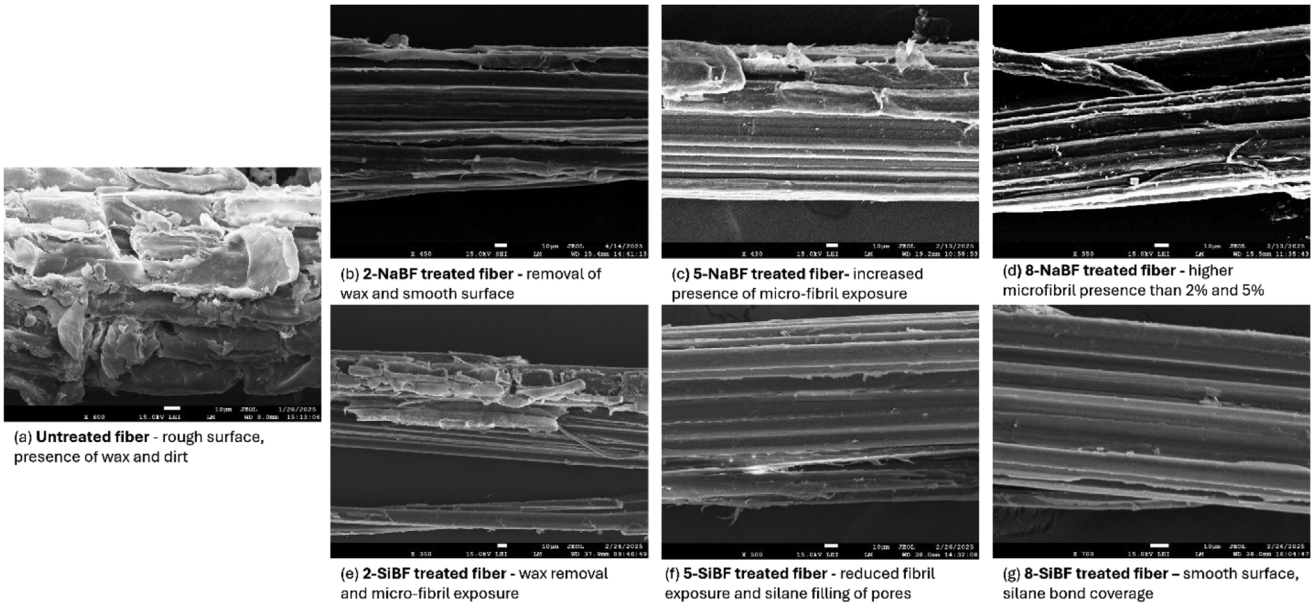

FIGURE 4 | SEM images of treated and untreated bamboo fibers with NaOH (b)–(d) and with Si (e)–(g) showing the morphological evolution after chemical treatment (scale bar corresponds to 10 μm).

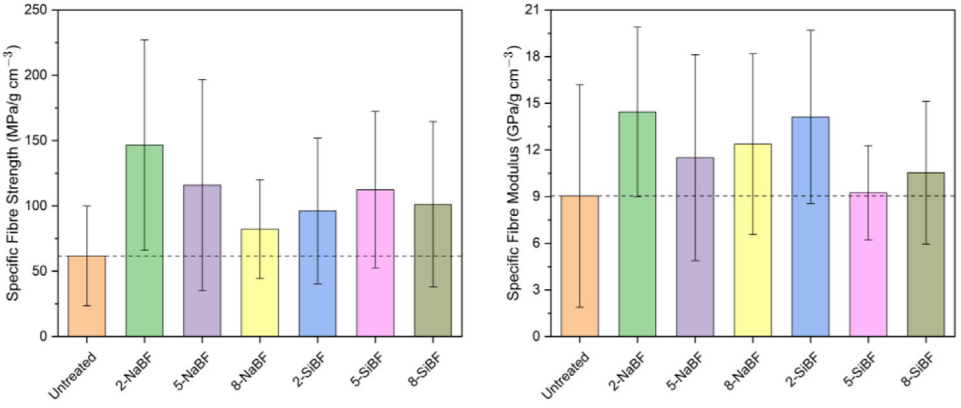

FIGURE 5 | Specific tensile properties of individual bamboo fibers.

TABLE 1 | Summary of Fiber Tensile Properties.

Property	Untreated	2-NaBF	5-NaBF	8-NaBF	2-SiBF	5-SiBF	8-SiBF
Strength (MPa)	110.64 ± 64.24	249.51 ± 129.28	205.92 ± 136.21	148.47 ± 64.22	161.70 ± 87.63	194.24 ± 98.18	168.06 ± 99.72
Elongation at Max Strength (mm)	0.71 ± 0.23	0.88 ± 0.28	0.89 ± 0.28	0.89 ± 0.36	0.54 ± 0.19	1.04 ± 0.40	0.85 ± 0.22
Modulus (GPa)	16.21 ± 12.10	24.59 ± 8.76	20.43 ± 11.16	22.34 ± 3.89	23.74 ± 8.76	15.99 ± 4.96	17.49 ± 7.24

33 g of usable film was obtained from 100 g of input, with significant loss due to bleed-out.

Mass-based stacking and symmetrical film placement ensured compositional uniformity, with fiber orientation alternated to balance trimmed stem offsets. The stack was preheated at 130°C (near PCs Tg) [30] for 30 min to soften fibers and allow minor realignment. Final consolidation was performed at 200°C and 5 bar, following the same protocol as for film preparation, ensuring consistency across laminates.

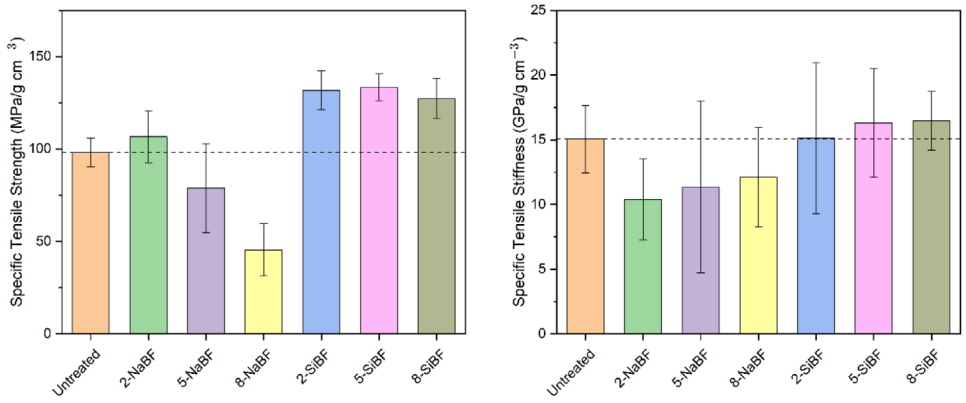

FIGURE 6 | Tensile Strength and Specific Tensile Stiffness of BF-PC composites.

3.7 | Composite Characterization Methods

Tensile testing was performed in accordance with ASTM D3039—*Standard Test Method for Tensile Properties of Polymer Matrix Composite Materials* [31]. Tests were conducted on a 20 kN Zwick universal testing machine equipped with a 20 kN load cell at a crosshead speed of 1 mm/min, as specified by the standard. Strain measurements were obtained using a clip-on extensometer mounted directly on the specimen surface.

Due to constraints in fiber length, the specimen dimensions were adapted within the permissible limits for unidirectional composites, with a total length of 140 mm and a width of 15 mm. A grip-to-grip gauge length of 90 mm was used to ensure proper clamping and prevent slippage. The chord modulus of elasticity was determined between strain values of 0.001 and 0.003, as recommended by ASTM D3039, using $E_{1a} = \Delta_\sigma/\Delta_\varepsilon$ with σ corresponding to stress and ε corresponding to strain.

The experimentally measured tensile properties were compared to predictions obtained via the Rule of Mixtures (RoM) to assess the efficiency of the composite reinforcement by calculating the bonding efficiency [32]. The longitudinal tensile modulus of the composite was estimated using the density-adjusted RoM:

$$E_{1t} = \frac{\left(\frac{E_f w_f}{\rho_f}\right) + \left(\frac{E_m w_m}{\rho_m}\right)}{\frac{w_f}{\rho_f} + \frac{w_m}{\rho_m}} \;\&\; E_m$$

$$= \left[\left\{E_{1a}\left(\frac{w_f}{\rho_f} + \frac{w_m}{\rho_m}\right)\right\} - \left(\frac{E_f w_f}{\rho_f}\right)\right] * \frac{\rho_m}{w_m}$$

where E_f is the fiber modulus, measured from the single fiber tensile tests, E_m is the matrix modulus, which was back-calculated using the experimentally determined tensile modulus E_{1a} of the laminate reinforced with untreated fibers and the RoM, ρ_f and ρ_m are the fiber and matrix densities, respectively, which were taken from the experimental measurements and w_f and w_m the fiber and matrix mass fraction, respectively, where for all calculations a fiber-to-matrix mass fraction of 40:60 was utilized. Given the processing conditions, the fibers or matrix did not undergo any thermal degradation and maintained constant properties. To isolate matrix-void effects, both the experimentally measured modulus and the Rule-of-Mixtures were normalized by their respective laminate densities, yielding the specific moduli.

$$\text{Specific } E_{1a} = \frac{E_{1a}}{\rho_a} \;\&\; \text{Specific } E_{1t} = \frac{E_{1t}}{\rho_t}$$

$$k = \frac{\text{Specific } E_{1a}}{\text{Specific } E_{1t}}$$

Flexural tests were conducted according to ASTM D7264–*Standard Test Method for Flexural Properties of Polymer Matrix Composite Materials* [33] using a 20 kN Zwick universal testing machine with a 1 mm/min crosshead speed. A four-point bending (4 PB) configuration was chosen over three-point bending to eliminate shear effects and ensure a constant bending moment. Due to laminate thickness variations, span lengths were adjusted based on a 32:1 span-to-thickness ratio. Failure modes—such as fiber pull-out, matrix cracking, and delamination were analyzed. Stress and strain were calculated using the standard equations:

$$\sigma = \frac{3PL}{4bh^2} \& \varepsilon = \frac{48\delta \mathrm{h}}{11L^2}$$

Mid-span deflection (δ) was derived from the displacement at the loading points as

$$\delta = \frac{3}{2}\,\delta_{nominal}$$

4 | Results and Discussion

4.1 | Fiber Studies

The influence of chemical treatment type and concentration on the skeletal density of fibers is shown in Figure 1. At lower concentrations (2%), both NaOH and silane treatments resulted in a reduction in skeletal density. This effect is attributed to the partial removal of lignin and surface waxes, which increases internal porosity. However, as NaOH concentration increased, more extensive delignification and wax

TABLE 2 | Summary of Composite Mechanical Properties.

	Untreated	2-NaBF	5-NaBF	8-NaBF	2-SiBF	5-SiBF	8-SiBF
Tensile							
Strength (MPa)	121.32 ± 8.59	124.80 ± 14.75	89.24 ± 24.34	49.31 ± 13.77	162.37 ± 11.61	161.79 ± 7.92	154.45 ± 11.75
Elongation at Max Strength (mm)	0.59 ± 0.09	0.61 ± 0.07	0.48 ± 0.10	0.71 ± 0.09	0.32 ± 0.06	0.50 ± 0.04	0.57 ± 0.08
Modulus (GPa)	18.62 ± 2.88	12.16 ± 3.28	12.85 ± 6.70	13.14 ± 3.74	18.63 ± 6.44	19.77 ± 4.54	19.99 ± 2.47
Flexural							
Strength (MPa)	154.20 ± 8.05	165.71 ± 7.80	126.15 ± 16.52	112.76 ± 19.71	184.89 ± 11.95	157.31 ± 7.00	154.00 ± 6.30
Modulus (GPa)	12.62 ± 1.24	10.97 ± 0.74	7.96 ± 0.93	10.17 ± 2.11	11.65 ± 1.77	10.30 ± 0.39	10.41 ± 0.93

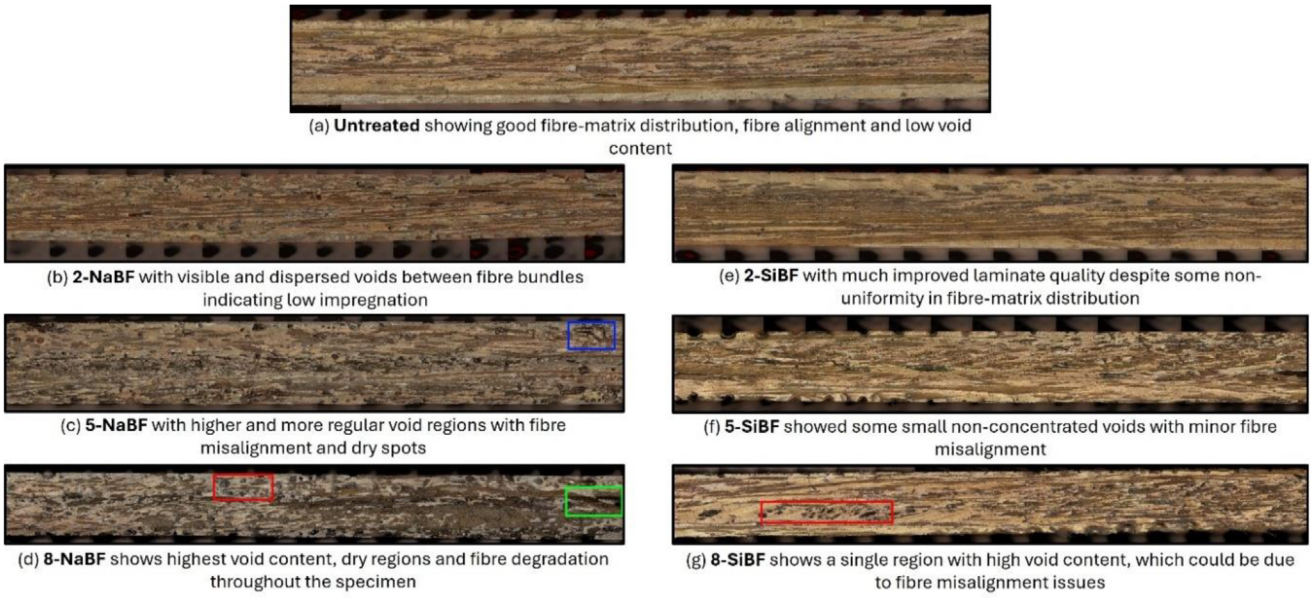

FIGURE 7 | Cross-sectional microscopy images of the laminates treated with NaOH (b)-(d) and with Si (e)-(g), highlighting voids (in red), misaligned and degraded fiber (in green), and entrapped moisture (in blue).

removal likely led to collapse of the internal pore structure and fiber compaction, thereby increasing the skeletal density [34]. A similar trend was observed with silane treatments, although the underlying mechanisms differ. The 5% silane treatment yielded the highest density among all silane concentrations, which may have contributed to pore filling and surface coating. At 8% silane, however, excessive degradation of binding components may have led to pore collapse and reduced the uniformity of silane coverage, slightly decreasing the density.

FTIR, density determination, and surface morphology of the fibers through SEM verified the chemical modifications induced by the treatments, as can be seen in Figures 2 and 3. The FTIR spectra of alkali-treated fibers exhibited notable changes indicative of lignin removal. A broad decrease in absorbance between 3500 and 2750 cm^{-1} corresponded to the reduction of O—H and C—H stretching vibrations, typically associated with lignin. Additionally, diminished intensity near 1600 cm^{-1}, corresponding to C═O and C═C functional groups, further supported the removal of lignin. Minimal changes were observed in other regions, suggesting that the alkali treatment selectively targeted lignin with limited impact on other fiber components.

In the case of silane-treated fibers, similar reductions in O—H and C—H bands were observed. However, the C═O region near 1600 cm^{-1} remained largely unchanged as no changes in lignocellulosic carbonyl groups are expected. Furthermore, new absorbance bands emerged around 1000 cm^{-1} (C—O—C vibrations) and between 1750 and 1000 cm^{-1}, corresponding to various Si—O and Si—C bonds. These

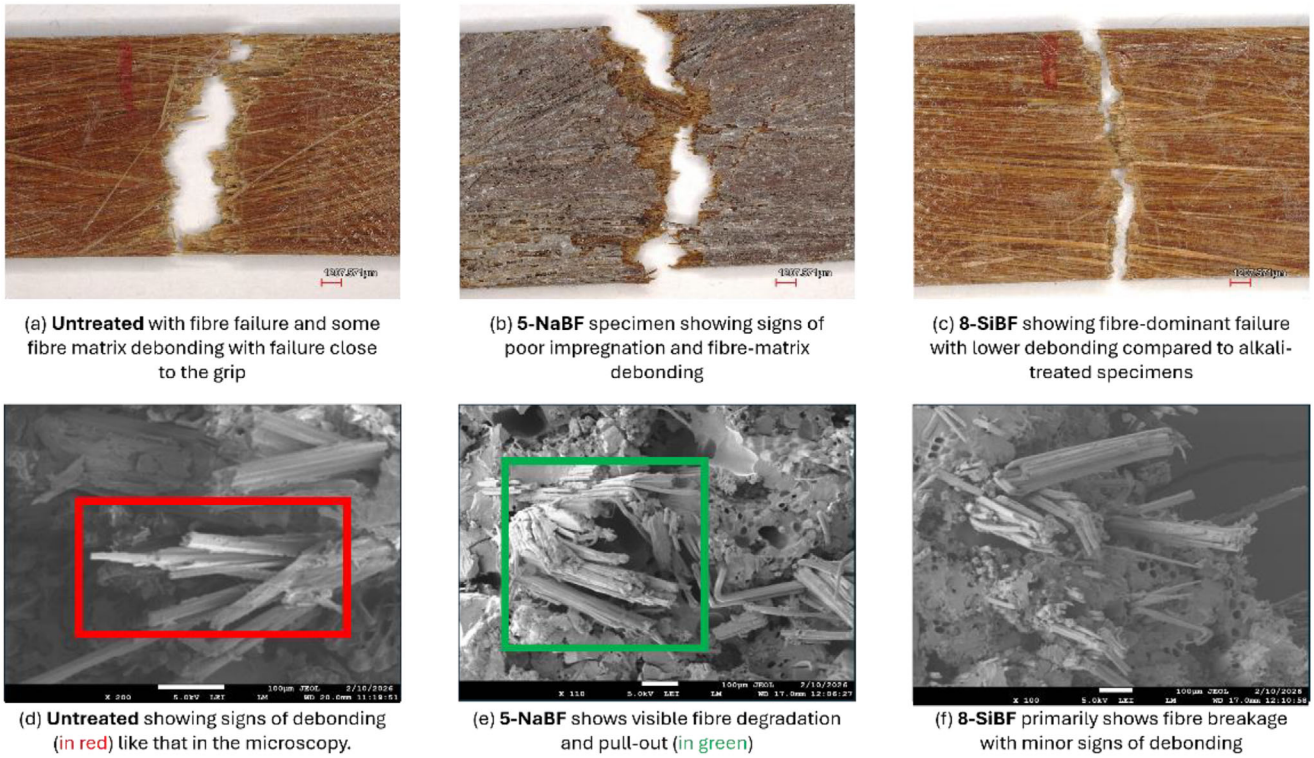

FIGURE 8 | Optical (scale bar corresponds to 1207 μm) and SEM images (scale bar corresponds to 100 μm) of fracture surfaces of tensile tested samples.

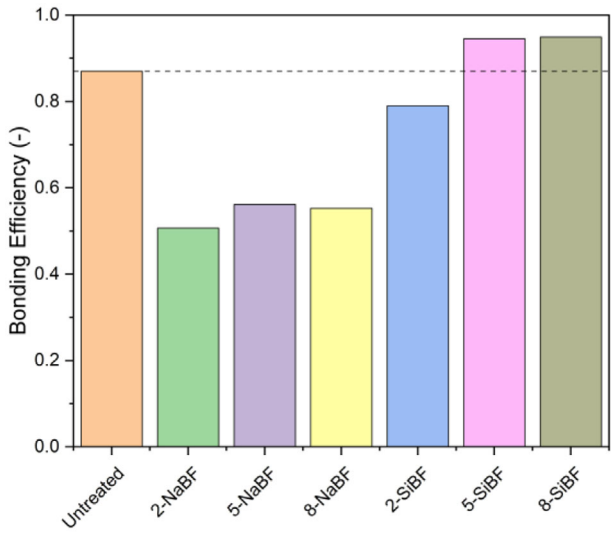

FIGURE 9 | Bonding Efficiency of BF-PC composites.

features confirm successful silane grafting onto the fiber surface.

Figure 4 shows the morphology of the fibers along the different treatments performed. Untreated fibers exhibited a rough, heterogeneous surface with visible surface impurities, waxes, and retained lignin, consistent with the typical morphology of lignocellulosic fibers [23]. Alkali treatment progressively enhanced surface smoothness with increasing NaOH concentration. At lower concentrations, partial delignification and superficial debris removal led to a visibly smoother surface. At higher concentrations, more extensive removal of lignin and waxes exposed the underlying microfibrillar structure, which increases surface area available for matrix interaction.

Silane treatment also induced notable morphological changes. At 2% concentration, partial removal of waxes and surface lignin was apparent, though surface heterogeneity persisted. In contrast, the 5% and 8% silane-treated fibers displayed smoother, more consolidated surfaces, with evidence of pore filling and a continuous silane-derived coating. This coating likely reduced the presence of exposed fibrils while promoting a chemically reactive interface.

Figure 5 presents the specific tensile properties of chemically treated bamboo fibers, normalized by skeletal density for direct comparison. Corresponding absolute values and fiber metrics are summarized in Table 1. All treatments led to improvements over the untreated baseline in both absolute and specific tensile properties.

2-NaBF showed the highest gains, attributed to partial removal of noncellulosic components, improved microfibril alignment, and reduced density from increased porosity. In 5-NaBF, although the absolute modulus remained high, increased fibrillation introduced defects and slightly raised density. At 8-NaBF, excessive degradation reduced both absolute and specific performance due to cellulose breakdown, microcracking, and pore collapse.

Silane-treated fibers also exhibit improved tensile properties, with 5-SiBF showing enhanced specific properties due to reduced

density and smoother fiber surfaces. However, 8-SiBF exhibited decreased performance, potentially due to brittle surface layers introduced by silane grafting.

4.2 | Composite Studies

The tensile strength and modulus of the composites were significantly influenced by chemical treatment type and concentration, as shown in Figure 6. Untreated laminates displayed a tensile strength of 121.3 MPa and a modulus of 18.62 GPa. All treated specimens exhibited a brittle failure mode under tensile loading, characterized by sudden fracture with the dominant failure mechanism being fiber fracture combined with partial fiber–matrix debonding. A slight improvement in tensile strength was observed for the 2-NaBF sample. However, higher concentrations (5% and 8%) led to a notable decrease in strength that falls below that of the untreated laminate. This decline aligns with an increase in void content, seen in Figure 10, as also evident in the specific tensile strength values—8-NaBF showed the poorest performance overall, with failure occurring predominantly along the fiber–matrix interface rather than within the fibers. In contrast, silane-treated laminates demonstrated enhanced tensile properties, particularly at 2% and 5% concentrations, and primarily exhibited fiber-dominated failure—an indication of better adhesion. The 2-SiBF sample exhibited the highest tensile strength, accompanied by a relatively low void content. Both 5-SiBF and 8-SiBF samples also retained high strength levels. Tensile modulus followed a similar trend. Silane-treated composites, especially 5-SiBF and 8-SiBF, achieved values approaching 20 GPa as seen in Table 2.

All specimens showed brittle failure with sudden fracture and nearly identical maximum and breaking loads. Most exhibited mixed fibre fracture and fibre–matrix debonding, while 8-NaBF showed dominant interfacial failure due to poor adhesion. Silane-treated samples displayed fibre-dominated failure, indicating improved bonding as seen in the microscopy and SEM imaging in Figure 7.

The bonding efficiency (BE) values for the various treatments can be seen in Figure 8. The untreated laminate shows a high BE, which is expected since the matrix modulus was back-calculated using the tensile modulus of this sample. Consequently, the experimentally measured modulus closely aligns with the theoretical Rule of Mixtures (ROM) prediction. The slight deviation is attributed to void content, which reduces the actual laminate density used in specific modulus calculations. Therefore, this BE value serves only as a reference baseline and not a true indicator of interfacial bonding for the untreated sample. Among the treated fibers, NaBF-treated laminates display significantly lower BE values reflecting weak fiber-matrix bonding. In contrast, SiBF-treated laminates demonstrate a steady increase in BE with higher silane concentrations. Notably, the 5-SiBF and 8-SiBF samples exhibit particularly high BE values, which arise from improved interfacial adhesion.

The flexural strength and modulus results, shown in Figure 9, further highlight the contrast between NaOH and silane treatments. The untreated laminate exhibited a flexural strength of 154.2 MPa and a modulus of 12.62 GPa. Treatment with 2% NaBF resulted in a slight increase in strength; however, higher concentrations led to a noticeable decline. This decrease correlates with increased void content, which likely compromises the matrix-dominated nature of flexural performance. In contrast, silane-treated laminates showed enhanced flexural strength, with a peak value of 184.89 MPa for the 2-SiBF sample. Although a slight reduction was observed at higher concentrations, both 5-SiBF and 8-SiBF maintained flexural strengths above 150 MPa as seen in Table 2. This improvement is attributed to enhanced fiber–matrix compatibility and better wetting afforded by the silane treatment, along with lower void content. Flexural modulus values, however, were generally lower for the treated specimens. This may suggest a more gradual load transfer between fiber and matrix as a result of the chemical treatments.

As seen in Figure 11, most flexural specimens fractured within the loading span, with silane-treated samples showing mainly fibre rupture and strong interfacial adhesion. NaOH-treated specimens, especially 5-NaBF and 8-NaBF, exhibited severe debonding and fragmented failures. Higher NaOH concentrations degraded the fibre-matrix interface.

5 | Conclusions

The integration of natural fibers with renewable polymer matrices is of critical importance to the circular composites industry. In this work, focus is placed on bamboo fibers and biobased polycarbonate matrix to manufacture sustainable composites, where fiber surface properties and process conditions are studied to monitor composite quality. At the fiber level, both alkali and silane treatments altered chemical functionality, density, and morphology, with notable improvements in tensile properties—especially at intermediate concentrations. Alkali treatment enhanced fibrillation and surface area but was highly sensitive to concentration, with higher NaOH levels compromising mechanical integrity.

At the composite level, silane-treated fibers consistently outperformed alkali-treated and untreated counterparts. The 2 g/L silane treatment emerged as the most effective, producing the highest tensile and flexural strengths (162 MPa and 184 MPa, respectively), reduced void content, and effective interfacial adhesion. These improvements were supported by increased bonding efficiency and more favorable fiber failure modes, suggesting successful chemical interactions at the fiber–matrix interface. In contrast, higher concentrations of alkali treatment led to fiber embrittlement, elevated void fractions, and diminished bonding efficiency.

Natural fiber surface functionalities play a crucial role in composite performance, especially at the interface level. In this case, bamboo fibers treated with silane offer a suitable route for biobased polycarbonate composite manufacturing through prepreg formation. We believe that so-formed composites are among the highest *Tg* natural fibre reinforced engineering thermoplastic composites reported in literature, and such advanced composites will pave the way for important applications such as circular aircraft interiors. This work serves as a vital contribution

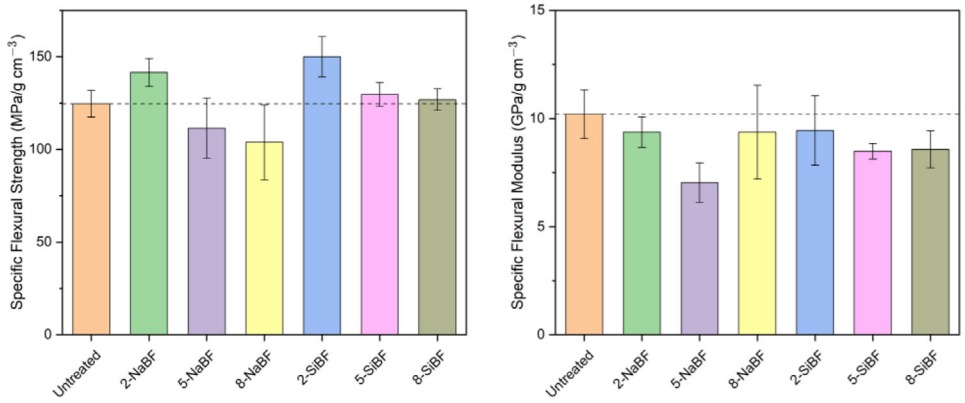

FIGURE 10 | Specific Flexural Strength and Specific Flexural Stiffness of BF-PC composites.

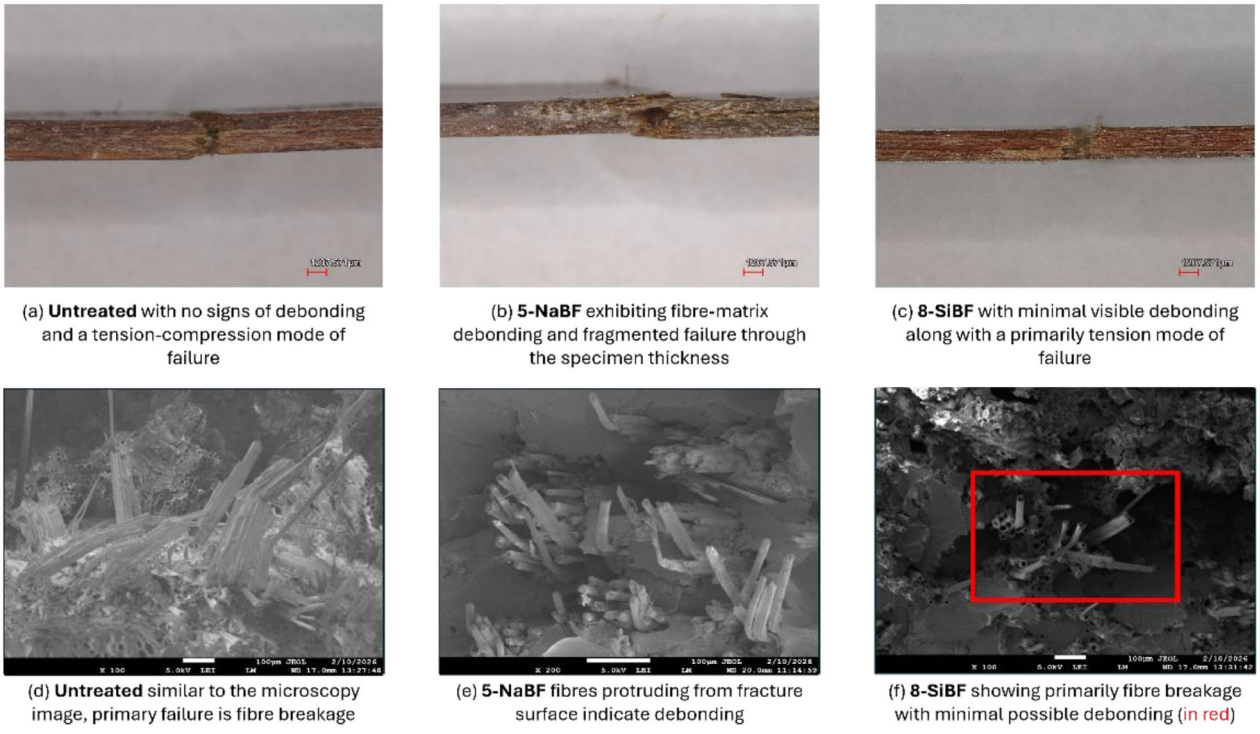

FIGURE 11 | Optical (scale bar corresponds to 1207 μm) and SEM (scale bar corresponds to 100 μm) images of fracture surfaces of flexural tested samples.

towards furthering the UN's Sustainable Development Goals 12 (Responsible consumption and production) and 13 (Climate Action) by promoting the use of bio-based, recyclable systems that can reduce dependence on fossil fuels and minimize the life-cycle greenhouse gas emissions.

Author Contributions

D.A., P.J., and B.K. conceived the study. P.J. developed the theoretical framework and performed the experiments. P.J. and D.A. aided in the analysis. B.K. supervised the project. All authors discussed the results and contributed to the final manuscript. D.A. and P.J. have equal contributions.

Acknowledgements

This project is made possible by a contribution and funding from Luchtvaart en Transitie. The authors acknowledge continuous support from the ASM department and technical staff. We extend our thanks to Mitsubishi Chemicals for supplying Durabio polymer pellets and Bambooder for their generous donation of bamboo fibres used in this study.

Conflicts of Interest

The authors declare no conflicts of interest.

Data Availability Statement

The data that support the findings of this study are available from the corresponding author upon reasonable request.

References

1. D. Apostolidis, W. E. Dyer, C. A. Dransfeld, and B. Kumru, "An Algae-derived Partially Renewable Epoxy Resin Formulation for Glass Fibre-reinforced Sustainable Polymer Composites," *RSC Applied Polymers* 2, no. 2 (2024): 149–154, https://doi.org/10.1039/d3lp00174a.

2. W. E. Dyer, P. Gupta, C. A. Dransfeld, N. Lorenz, and B. Kumru, "Formulating Brown Algae Derived Phloroglucinol-Based Epoxy Resin for High Performance Applications," *ACS Applied Polymer Materials* 6 (2024): 13371–13377, https://doi.org/10.1021/acsapm.4c02804.

3. J. Bachmann, X. Yi, H. Gong, et al., "Outlook on Ecologically Improved Composites for Aviation Interior and Secondary Structures," *CEAS Aeronautical Journal* 9, no. 3 (2018): 533–543, https://doi.org/10.1007/s13272-018-0298-z.

4. J. Bachmann, X. Yi, K. Tserpes, et al., "Towards a Circular Economy in the Aviation Sector Using Eco-composites for Interior and Secondary Structures. Results and Recommendations from the eu/china Project eco-compass," *Aerospace* 8, no. 5 (2021): 131, https://doi.org/10.3390/aerospace8050131.

5. V. Yaghoubi and B. Kumru, "Retrosynthetic Life Cycle Assessment: a Short Perspective on the Sustainability of Integrating Thermoplastics and Artificial Intelligence into Composite Systems," *Advanced Sustainable Systems* 8, no. 5 (2024): 2300543, https://doi.org/10.1002/adsu.202300543.

6. J. J. Andrew and H. N. Dhakal, "Sustainable Biobased Composites for Advanced Applications: Recent Trends and Future Opportunities—A Critical Review," *Composites Part C: Open Access* 7 (2022): 100220, https://doi.org/10.1016/j.jcomc.2021.100220.

7. H. P. S. Abdul Khalil, I. U. H. Bhat, M. Jawaid, A. Zaidon, D. Hermawan, and Y. S. Hadi, "Bamboo Fibre Reinforced Biocomposites: A Review," *Materials & Design* 42 (2012): 353–368, https://doi.org/10.1016/j.matdes.2012.06.015.

8. D. Beaumann, Material Characterisation of Mechanically Extracted Continuous Bamboo Fibre Reinforced Polymers, 2024, https://repository.tudelft.nl/record/uuid:03ad1d9e-fed4-460a-8b1c-8f92220d2e0a.

9. P. Jayaraman and S. Hegde, "Influence of Fly-ash Filler and Moisture Content on Vibrational and Acoustic Properties of Basalt Fibre Reinforced Composites," *Advances in Materials and Processing Technologies* 11, no. 2 (2025): 1072–1084, https://doi.org/10.1080/2374068X.2024.2357935.

10. H. P. S. Abdul Khalil, I. U. H. Bhat, M. Jawaid, A. Zaidon, D. Hermawan, and Y. S. Hadi, "Bamboo Fibre Reinforced Biocomposites: A Review," *Materials & Design* 42 (2012): 353–368, https://doi.org/10.1016/j.matdes.2012.06.015.

11. M. M. Kabir, H. Wang, K. T. Lau, and F. Cardona, "Chemical Treatments on Plant-Based Natural Fibre Reinforced Polymer Composites: An Overview," *Composites Part B: Engineering* 43, no. 7 (2012): 2883–2892, https://doi.org/10.1016/j.compositesb.2012.04.053.

12. B. T. Wagaye, J. Guo, B. Zhou, C. Gao, and L. T. Nguyen, "Surface Modification of Plain-Woven Ramie Fabrics Using Bridged Bis (3-Trimethoxysilylpropyl) Amine Silane for Improved Hydrophobicity," *Fibers and Polymers* 25, no. 11 (2024): 4307–4320, https://doi.org/10.1007/s12221-024-00737-8.

13. V. Deepak, L. G. Kheng, and V. Vrince, "Interfacial Studies of Natural Fiber-Reinforced Particulate Thermoplastic Composites and Their Mechanical Properties," *Journal of Natural Fibers* 19, no. 6 (2022): 2299–2326, https://doi.org/10.1080/15440478.2020.1808147.

14. O. Vetterli, G. A. Pappas, and P. Ermanni, "Effects of Processing on the Mechanical Performance of GF-PC Composites: a Multiscale Investigation," *Polymer Composites* 47 (2025): 1300–1315, https://doi.org/10.1002/pc.70218.

15. D. Kyriacos, *Brydson's Plastics Materials: Eighth Edition* (Elsevier Inc., 2017), 457–485, https://doi.org/10.1016/B978-0-323-35824-8.00017-7.

16. J. Zhang, A. Koubaa, D. Xing, et al., "High-performance Lignocellulose/Polycarbonate Biocomposites Fabricated by in Situ Reaction: Structure and Properties," *Composites Part A: Applied Science and Manufacturing* 138 (2020): 106068, https://doi.org/10.1016/j.compositesa.2020.106068.

17. D. Apostolidis, P. Jayaraman, C. A. Dransfeld, B. Kumru, and N. Lorenz, "Linking Process-Induced Degradation to Mechanical Property Deterioration in Flax Fiber–Reinforced Bio-Polymer Matrix Composites," *Polymer Composites* (2026), https://doi.org/10.1002/pc.70765.

18. C. U. Maheswari, K. O. Reddy, E. Muzenda, and A. V. Rajulu, "Tensile and Thermal Properties of Polycarbonate-Coated Tamarind Fruit Fibers," *International Journal of Polymer Analysis and Characterization* 17, no. 8 (2012): 578–589, https://doi.org/10.1080/1023666X.2012.718527.

19. J. Zhang, A. Koubaa, D. Xing, et al., "High-performance Lignocellulose/Polycarbonate Biocomposites Fabricated by in Situ Reaction: Structure and Properties," *Composites Part A: Applied Science and Manufacturing* 138 (2020): 106068, https://doi.org/10.1016/j.compositesa.2020.106068.

20. F. J. Alonso-Montemayor, D. Á. Navarro-Rodríguez, M. Delgado-Aguilar, et al., "Plasma-Treated Lignocellulosic Fibers for Polymer Reinforcement. A Review," *Cellulose* 29 (2022), 659–683, https://doi.org/10.1007/s10570-021-04361-0.

21. V. Antonelli, Improvements of Thermoforming of Thermoplastic Composites Using a Collection of Rubber Particles as a Soft Mould Half Experiments and Modelling, (2014).

22. Standard Test Methods for Density Determination of Flax Fiber, ASTM International, 2018, http://www.astm.org/cgi-bin/resolver.cgi?D8171-18.

23. A. Kudva, G. T. Mahesha, and D. Pai, "Influence of Chemical Treatment on the Physical and Mechanical Properties of Bamboo Fibers as Potential Reinforcement for Polymer Composites," *Journal of Natural Fibers* 21, no. 1 (2024): 2332698, https://doi.org/10.1080/15440478.2024.2332698.

24. G. Hu, S. Cai, Y. Zhou, N. Zhang, and J. Ren, "Enhanced Mechanical and Thermal Properties of Poly (lactic acid)/Bamboo Fiber Composites via Surface Modification," *Journal of Reinforced Plastics and Composites* 37, no. 12 (2018): 841–852, https://doi.org/10.1177/0731684418765085.

25. P. Nguyen Tri, C. Sollogoub, and A. Guinault, "Relationship between fiber Chemical Treatment and Properties of Recycled Pp/Bamboo Fiber Composites," *Journal of Reinforced Plastics and Composites* 29, no. 21 (2010): 3244–3256, https://doi.org/10.1177/0731684410370905.

26. K. Vishal, A. Arun, and K. Rajkumar, "Extraction and Characterization of Steam-Exploded Silane-Treated Cellulosic Natural Vernonia Elaeagnifolia Long Fibre," *Industrial Crops and Products* 214 (2024): 118576, https://doi.org/10.1016/J.INDCROP.2024.118576.

27. T. Lu, M. Jiang, Z. Jiang, D. Hui, Z. Wang, and Z. Zhou, "Effect of Surface Modification of Bamboo Cellulose Fibers on Mechanical Properties of Cellulose/Epoxy Composites," *Composites Part B: Engineering* 51 (2013): 28–34, https://doi.org/10.1016/J.COMPOSITESB.2013.02.031.

28. Standard Test Method for Tensile Strength and Young's Modulus of Fibers, https://store.astm.org/c1557-20.html.

29. L. A. Bosworth and S. Downes, "Acetone, a Sustainable Solvent for Electrospinning Poly(ε-Caprolactone) Fibres: Effect of Varying Parameters and Solution Concentrations on Fibre Diameter," *Journal of Polymers and the Environment* 20, no. 3 (2012): 879–886, https://doi.org/10.1007/s10924-012-0436-3.

30. J. Baltscheit, N. Schmidt, F. Schröder, and J. Meyer, "Investigations on the Aging Behavior of Transparent Bioplastics for Optical Applications," *InfoMat* 2, no. 2 (2020): 424–433, https://doi.org/10.1002/inf2.12065.

31. D 3039/D 3039M-00 Standard Test Method for Tensile Properties of Polymer Matrix Composite Materials, https://store-astm-org.tudelft.idm.oclc.org/d3039_d3039m-08.html.

32. W. Woigk, C. A. Fuentes, J. Rion, et al., "Interface Properties and Their Effect on the Mechanical Performance of Flax Fibre Thermoplastic Composites," *Composites Part A: Applied Science and Manufacturing* 122 (2019): 8–17, https://doi.org/10.1016/J.COMPOSITESA.2019.04.015.

33. D 7264/D 7264M-07 Standard Test Method for Flexural Properties of Polymer Matrix Composite Materials, https://store-astm-org.tudelft.idm.oclc.org/d7264_d7264m-21.html.

34. R. D. Murwamadala, L. B. Mathebela, and M. P. Mubiayi, "Impact of Alkali Treatment on the Internal Microstructure, Surface Topography and the Resulting Mechanical Properties of Single Sisal Fibers," *Journal of Natural Fibers* 21, no. 1 (2024): 2370028, https://doi.org/10.1080/15440478.2024.2370028.